Marine Geophysical Research (2020) 41:21
https://doi.org/10.1007/s11001-020-09421-x

ORIGINAL RESEARCH PAPER

Multi-attribute machine learning analysis for weak BSR detection in the Pegasus Basin, Offshore New Zealand

Julian Chenin[1] · **Heather Bedle**[1]

Received: 10 April 2020 / Accepted: 20 October 2020

Abstract

Gas hydrates that exist in the subsurface are often difficult to detect with reflection seismic data if the seismic data lacks a strong bottom simulating reflection (BSR). In these cases, the imaging and detection of the gas hydrate stability zone (GHSZ) becomes particularly difficult, as hydrate detection relies heavily on the BSR, gas chimneys, or pockmarks on the seafloor. To address and improve upon these imaging complications, an unsupervised machine learning multi-attribute analysis is performed on 2D seismic data in the Pegasus Basin in New Zealand where the BSR is not continuously or clearly imaged. Rock physics analysis has demonstrated that the inclusion of methane gas hydrates in the pore space results in a slightly increasing amplitude at the base of the gas hydrate zone, regardless of the fluid (brine or gas) in the pore space below the hydrates. This increasing amplitude is quite weak and can be masked by noise. In the scenarios where a strong seismic impedance difference is lacking, a BSR is not typically observed in the seismic data, even though gas hydrates do exist in the subsurface. To enhance the detection of the presence of gas hydrates, a multi-attribute analysis is performed with a series of seismic attributes that can detect the minute changes in the seismic waveform due to the presence of gas hydrates. The successful attributes are those that are sensitive to attenuation, frequency, and small amplitude anomalies.

Keywords Offshore · Seismic · Hydrates · Interpretation · Machine learning

Introduction

Gas hydrates (sometimes referred to as clathrate hydrates) are solid solutions where a host lattice is created though water molecules linking together via hydrogen bonding to enclose a diverse variety of molecules, most commonly methane (Englezos 1993). The formation of gas hydrates is only possible in high-pressure and low temperature environments such as permafrost and the shallow subsurface beneath continental slopes, including below the continental slope, offshore New Zealand (Katz 1981, 1982; Riedel et al. 2010). While gas hydrates exist globally, there are no reliable and universal methods to identify their presence in the subsurface. Bottom simulating reflectors (BSRs) are the most common method of identifying hydrates in seismic data; as has been done in the Ulleung Basin within the East Sea, in the Krishna-Godavari Basin within the Bay of Bengal, and in the Blake Ridge, offshore South Carolina (Holbrook et al. 1996; Yoo et al. 2013; Dewangan et al. 2014). These BSRs are present at the base of the gas hydrate stability zone (GHSZ), which tends to parallel the seafloor due to the pressure and temperature requirements for gas hydrate stability. BSRs are identified by looking for high amplitude reflections that cross stratigraphy and are caused by a sharp decrease in acoustic impedance in the rocks as the hydrates transition from their solid form, to a free gas form due to changing pressure and temperature conditions with depth beneath the seafloor (Singh et al. 1993; Ecker et al. 2000; Griffin et al. 2015). Because of the underlying free gas, the BSRs will have a large negative reflection coefficient due to a decrease in the P-wave velocity (Navalpakam et al. 2012). However, BSRs are not always observed in areas where gas hydrates are believed to be present (e.g. Finley and Krason 1988; Wood and Ruppel 2000; He et al. 2006). Two key reasons for weak BSRs are probably due to (1) not enough free gas below the hydrate to create the needed impedance contrast or (2) stratigraphy-parallel BSRs that are subtle and can only be identified with advanced seismic analysis (Xu and Ruppel 1999; Plaza-Faverola et al. 2012). In these cases,

✉ Julian Chenin
julian.chenin@ou.edu

[1] School of Geosciences, University of Oklahoma, Norman, OK, USA

Published online: 06 November 2020

the imaging and detection of the gas hydrate stability zone (GHSZ) becomes particularly difficult, since hydrate detection relies heavily on a large decrease in acoustic impedance due to a significant drop in P-wave velocity resulting from trapped gas below the BSR (Singh et al. 1993; Navalpakam et al. 2012). Additional methods to support the presence of hydrates include gas chimneys, or pockmarks on the seafloor that are indicative of gas migration (Plaza-Faverola et al. 2012). These 'missing' BSRs demonstrate that an improved understanding of the expected seismic response is needed in areas where no other hydrate identifier is present.

As BSRs are used to infer the presence of hydrates, it becomes difficult to infer the presence of hydrates where robust BSRs are lacking (Riedel et al. 2010). A clear BSR is observed through most of the Pegasus Basin, offshore New Zealand, but is observed to be weak, discontinuous, or absent in some regions. Therefore, do hydrates exist where no BSRs are present within the GHSZ, or are there no hydrate accumulations in these regions? This research question is highlighted in Fig. 1a, b where a section of weak amplitude BSRs are separated by two, distinct high amplitude BSRs in Line 19 of the PEG09 seismic survey. There is a high amplitude contrast where high amplitude BSRs are observed due to the trapped free gas below the hydrate accumulations (Fig. 1b-1). However, where there is no trapped free gas to create a high amplitude contrast, there could still be hydrates present. In these areas, a small amplitude contrast would still be observed (Fig. 1b-2), however, not as pronounced compared to the surrounding background amplitude responses due to lithology interfaces such as in Fig. 1b-3. This figure highlights the relationship between acoustic impedance contrasts resulting from varying amounts of hydrate accumulations.

There are several motivations for better quantifying gas hydrate volumes in the subsurface as gas hydrates can serve as an economic resource as well as a geohazard. Hydrates can serve as an economic resource as they have the capability of behaving as a seal for conventional hydrocarbon reservoirs (Singh et al. 1993; Makogon et al. 2007; Walsh et al. 2009). They are also a geohazard, as sediments which contain gas hydrates can be destabilized through natural or man-made events eventually triggering landslides (Field and Barber 1993; Faure et al. 2009).

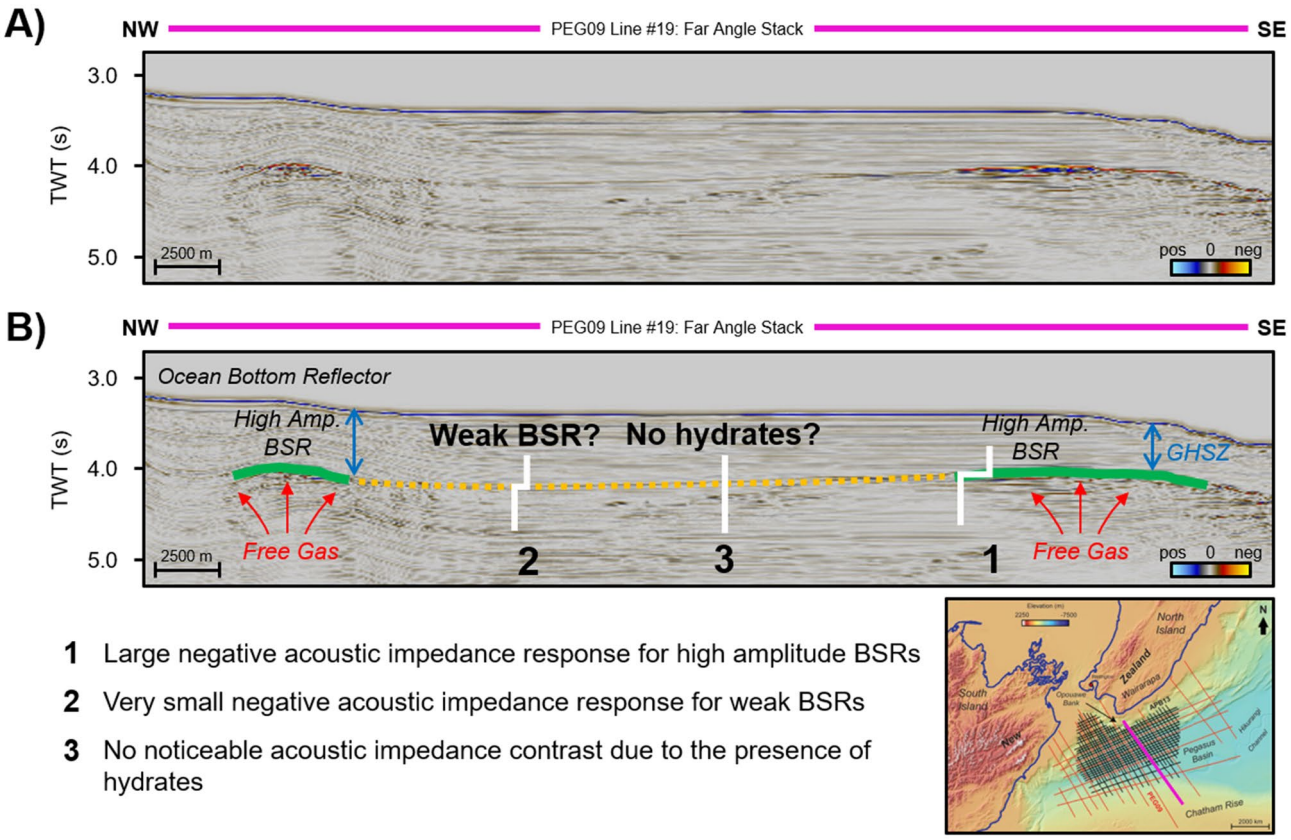

Fig. 1 **a** Cropped far angle stack seismic amplitude section of Line 19 from the PEG09 survey with **b** an interpreted section highlighting the expected amplitude responses for high amplitude BSRs, weak BSRs and for regions with no BSR. This figure also provides a reference where the base of the gas hydrate stability zone (GHSZ) is and why high amplitude BSRs have a large acoustic impedance contrast resulting from the trapped free gas below. Bathymetry map taken from the General Bathymetric Chart of the Oceans (GEBCO) Compilation Group (2019)

Pegasus Basin

Geologic background

The Pegasus Basin, located offshore New Zealand, lies between two subduction systems with the Hikurangi Margin and the East Coast Basin to the northwest and the extinct subduction of the Chatham Rise to the southeast (Fig. 2a–c) (Plaza-Faverola et al. 2012; Kroeger et al. 2015). The formation of the basin is controlled by the convergence between the Australian and Pacific Plates (Kroeger et al. 2015). The Hikurangi Margin, offshore eastern Wairarapa, is a sediment-rich active continental margin that is related to the westward subduction of the Pacific Plate beneath New Zealand's continental crust, where faulting transitions from subduction to oblique-slip (Plaza-Faverola et al. 2012; Kroeger et al. 2015).

The southern part of the imbricated accretionary wedge of the overriding Australian Plate extends 40 km off southeastern Wairarapa, where it gives way to the southern Hikurangi Trough (Pegasus Basin). The Pegasus Basin has an approximate water depth of 1000 to 2600 m but can exceed 3000 m along the Hikurangi Channel. Deeper water generally marks the location of the modern plate interface where the Hikurangi Plateau is subducting under the North Island of New Zealand, however, this is not as apparent in the Pegasus Basin except towards the north (Plaza-Faverola et al. 2012; Kroeger et al. 2015; Bland et al. 2015). From Neogene to modern time, approximately 6 km of clastic deposits have filled the basin sourced by the erosion of the uplifted North Island and thins southwards towards the Chatham Rise (Kroeger et al. 2015). A prominent geomorphologic feature in the Pegasus Basin is the Miocene-age Hikurangi Channel, a 2000 km long aggradational deep-sea channel which runs almost parallel to the accretionary prism. It is sourced from the south-west by the Southern Alps uplift and flows along the northern slope of the Chatham Rise (Lewis et al. 1998; Kroeger et al. 2015).

Hydrates in the Pegasus Basin

Gas hydrates have formed in sediments of Pliocene to modern age, occupying the shallowest portion of the basin at water depths greater than 600 m within the Pegasus Basin (Navalpakam et al. 2012; Kroeger et al. 2015). In order for these gas hydrates to form, there are three dominant

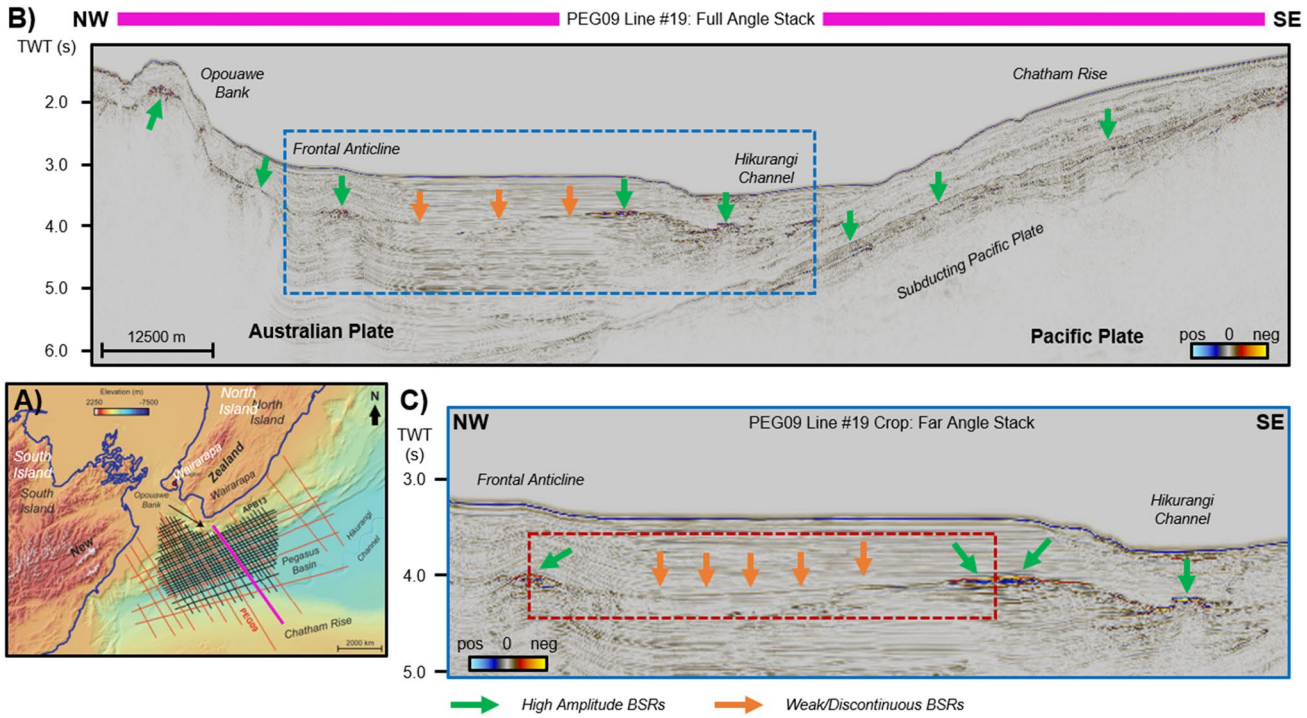

Fig. 2 **a** Study area within the Pegasus Basin, offshore New Zealand. The PEG09 2D survey is denoted in red while the more recent APB13 2D survey is shown in black. **b** The entire 2D vertical full angle stack seismic profile of Line 19 from the PEG09 survey, further highlighting key geologic structures and types of BSRs. **c** Takes a closer look at the far angle stacks for Line 19 to show the weak/discontinuous BSRs versus the high amplitude BSRs. The far angle stacks helped to better visualize some of the weaker BSRs and further infer the presence of hydrates. The red box shown here references the amplitude section studied in Fig. 6. Bathymetry map taken from the General Bathymetric Chart of the Oceans (GEBCO) Compilation Group (2019)

geological controls on the thickness of the free-gas zone, as well as the free gas underlying gas hydrates: (1) the rate of upward fluid flow relative to the seabed, (2) the pressure and temperature conditions at the base of the GHSZ, and (3) tectonic uplift rate of the seabed (Haacke et al. 2007). Recent studies suggest that the hydrates in the Pegasus Basin are sourced from Quaternary microbial methane and upward migration of gas from beneath the GHSZ (Plaza-Faverola et al. 2012; Kroeger et al. 2015). The migration pathways for the gas were along fault planes and laterally from less permeable hydrate bearing zones to more permeable areas (Henrys et al. 2009; Plaza-Faverola et al. 2012, Kroeger et al. 2015).

There are three primary zones where hydrates are sustained by focused fluid migration pathways and concentrated within the Pegasus Basin (Plaza-Faverola et al. 2012): close to the New Zealand shore along the Opouawe Bank, at the crest of the frontal anticline, and in the sands beneath the Hikurangi Channel (Fig. 2b). A clear BSR is observed through most of the basin, but in some regions is observed to be weak, discontinuous, or absent (Fig. 2b, c). Previous studies have linked clear BSRs to geological structures that promote fluid flow, such as anticlines or faults (Henrys et al. 2009; Plaza-Faverola et al. 2012; Crutchley et al. 2019). There are also instances where hydrates can fill open pores and fractures locally, thus creating a permeability barrier and causing free gas to migrate laterally towards structural highs (Nimblett and Ruppel 2003). Therefore, a majority of the weak BSRs in this study area are located where strata is laterally continuous with no significant degree of dip yet high amplitude BSRs are observed where anticlinal features or other migration pathways are present.

Data

Within the Pegasus Basin, this study analyzes two 2D seismic datasets: the PEG09 and APB13 surveys (Fig. 2a-c). There are no wells currently drilled in the Pegasus Basin. The PEG09 survey consists of several long-offset, multichannel seismic 2D profiles that cover approximately 3200 km and were collected in 2009. This survey was contracted by the New Zealand Ministry of Economic Development and shot by RV Reflect Resolution (now RPS Energy), between November 2009 and March 2010, to stimulate exploration interest within the basin as it showed promising petroleum potential (Bland et al. 2015). The record length was 12 s using a 2 ms sampling rate and was processed by Gardline CGG PTE Ltd. This survey was later reprocessed by CGG Services in Singapore under contract to Anadarko New Zealand Company in 2014 (Anadarko New Zealand 2014a; b). The more recent APB13 survey was similarly acquired and processed in 2014 by CGG Services in Singapore and also consists of wide-angle, multichannel seismic 2D profiles covering 4600 km. The recording length was 10.5 s using a 2 ms sampling rate. Both datasets are positive standard polarity with a shot interval of 37.5 and a group interval of 12.5 m (Anadarko New Zealand 2014a; b). Both high and weak amplitude BSRs exist within both surveys, shown in Fig. 3a, b as an example. These line pairs were chosen as they are from two different 2D surveys yet show similar high amplitude and weak/discontinuous BSRs.

Figures 3a, b highlight a similar N–S vertical seismic profile from both 2D seismic datasets in the Pegasus Basin. In both lines, there are a few distinct, high-amplitude BSRs that are indicative of gas hydrates. Figures 3c, d take a closer look between the two high-amplitude BSRs from Fig. 3a, b, respectively. The BSRs' amplitude responses appear to dim horizontally between one another, reducing confidence in the interpretation that hydrates are present in this region. The dim, horizontal amplitude response between both strong BSRs imaged at each end of the line is interpreted to be a weak BSR which begs the question of whether a BSR is a sufficient condition for hydrates to exist? Are there also hydrates where the BSR is not clear and is discontinuous (Hillman et al. 2017; Bedle 2019)? Furthermore, is there a method for better characterizing stratigraphy parallel BSRs? Are the BSRs actually there, but very subtle? Or are the BSRs not there? Previous studies have linked high amplitude BSRs to geological structures such as anticlines and faults which promote fluid flow (Henrys et al. 2009; Plaza-Faverola et al. 2012; Crutchley et al. 2019). However, in laterally continuous areas with no significant dip, it is difficult for free gas to become trapped underneath and create high-amplitude BSRs. The lack of trapped free gas to create a strong impedance contrast beneath the weak BSRs makes it difficult to determine if there is hydrate present there or not. Traditional geophysical gas hydrate identifications methodologies need to be further improved as they are limited in answering these questions. Previous studies conducted some rock-physics modeling analyses to further investigate the seismic response of gas hydrates (Dvorkin and Nur 1996; Dvorkin et al. 1999; Dvorkin et al. 2003; Bedle 2019).

Gas hydrate stability zone (GHSZ)

Previous rock physics modeling analyses have demonstrated that the inclusion of methane gas hydrates in the pore space results in a slightly increased amplitude at the base of the gas hydrate zone, regardless of the fluid (brine or gas) in the pore space below the hydrates (Spence et al. 2010; Lui and Lui 2018). However, laboratory results show that the Vp of the sediments with hydrate increases only after saturation reaches approximately 40% and the hydrate starts to cement the grains (Yun et al. 2007; Waite et al. 2009). This increased amplitude is quite weak in strength, particularly in shale rich lithologies, or in sandier lithologies where the

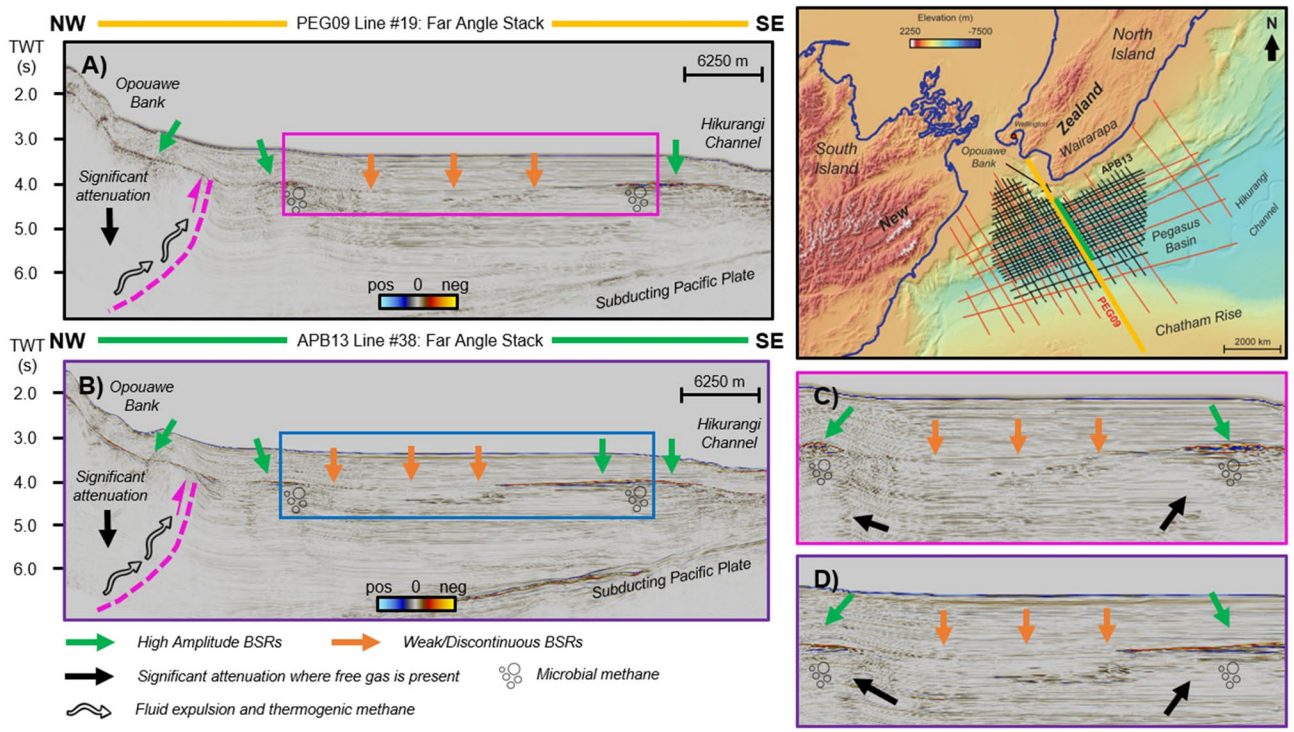

Fig. 3 **a** PEG09 Line 19, **b** APB13 Line 38 within the Pegasus Basin, offshore New Zealand. These lines were chosen as they are from two different surveys yet are the closest to each other. **c** A zoomed in portion of PEG09 Line 19 to highlight the difference between high amplitude BSRs (shown by the green arrows) and the weak/discontinuous BSRs (shown by the orange arrows). **d** A zoomed in portion of the APB13 Line 38 also highlighting the difference between high amplitude and weak/discontinuous BSRs. Both surveys show similar high amplitude and weak/discontinuous BSRs. The fluid expulsion and thermogenic methane migration pathways are also shown along with the significant seismic attenuation (black arrows) created from trapped free gas, migrations pathways containing free gas and complex faulting zones (Horizons and faults were modified from Kroeger et al. 2015 and interpreted on a time volume). Fluid expulsion, thermogenic methane pathways and microbial methane modified after Henrys et al. (2009), Plaza-Faverola et al. (2012) and Kroeger et al. (2015). Bathymetry map taken from the General Bathymetric Chart of the Oceans (GEBCO) Compilation Group (2019)

pore space contains brine. The seismic wavefield is particularly sensitive to the active migration of free gas, causing amplitude blanking due to significant attenuation (Guerin et al. 1999; Dewangan et al. 2014). This attenuation is well highlighted in Fig. 3a, b where the faults become very difficult to image due to the significant attenuation caused by the migration of free gas, a complex faulting system and depth of signal penetration (Dewangan et al. 2014). However, in the instance of hydrate-bearing sediments with no trapped free gas underneath, there appears to be low attenuation when compared to the attenuation of background sediments (Dewangan et al. 2014). Significant attenuation is therefore only expected where trapped free gas is present (Guerin et al. 1999; Dewangan et al. 2014) and no significant attenuation is observed for hydrate-bearing sediments with no trapped free gas beneath them. This attenuation effect caused by trapped free gas is clearly shown between the two high-amplitude BSRs from Fig. 3c, d. Large saturations of hydrate within the rock will cause P- and S-wave velocities to increase substantially relative to the same rock with no hydrate inclusions within the pore space (Dvorkin et al. 2003; Spence et al. 2010). However, for small concentrations of hydrate within the rock, it becomes more difficult to observe this effect, especially as it relates to S-waves. This velocity increase depends on how the hydrates are distributed at the grain scale as S-wave velocities depend on the rigidity and shear modulus of the host rock (Yun et al. 2005, 2007; Spence et al. 2010; Kim et al. 2013).

Bedle (2019) formulated a series of rock-physics models to evaluate how various elastic properties change with different hydrate saturations and mediums. From these hydrate rock-physics models, amplitude versus angle (AVA) responses can be derived. This is important because AVA attributes can now be calculated to potentially better reveal the extent of the GHSZ. Bedle (2019) demonstrated that a Class 3 AVA response (low intercept value and a negative gradient where amplitude becomes increasingly more negative at larger angles) is observed for hydrocarbon accumulations where high amplitude BSRs are present (Chopra and Castagna 2014). In the instance of brine, a very weak Class 2n AVA response (has a low intercept value and a negative gradient where the amplitude becomes more negative

at larger angles) is expected whether the BSR exists in a sand or shale (Chopra and Castagna 2014; Bedle, 2019). Therefore, the rock-physics modeling demonstrates that in regions where hydrocarbons (or biogenic gas in our study area) are not at significant enough saturation to cause a seismic anomaly, such as laterally in between high amplitude BSRs, hydrates would be best detected in the far angle stack because in these regions because the expected seismic response is a Class 2n AVA.

Several AVA attributes were then used to further identify the extent of hydrates in the Pegasus Basin. Bedle (2019) found that these attributes further increased ability to identify some previous seismically invisible BSRs. However, can this identification method be further improved to identify the full extent of the GHSZ? We have developed a new methodology, which uses an unsupervised machine learning multi-attribute analysis on 2D, full- and angle- stack seismic data within the Pegasus Basin with self-organizing maps (SOMs) is employed to better detect these seismically invisible/weak BSRs.

Methodology

Although AVA attributes help to enhance the extent of hydrates in the seismic data, individual attributes are limited in revealing their entire presence. Each attribute will highlight different properties of the BSRs, and an iterative interpretation process is needed to capture the total extent of the hydrates. However, by using a machine learning approach that incorporates all of these attributes, this iterative attribute interpretation workflow can be eliminated. The machine learning model can instead combine multiple attributes into one comprehensive attribute to highlight the extent of hydrates. This study uses principle component analysis (PCA) to analyze the multi-dimensional nature of these attribute combinations and visualizes these relationships using SOMs. There have been multiple geophysical studies using PCA and SOMs to better characterize the subsurface. Sacrey and Roden (2014) looked at several conventional and unconventional case studies to demonstrated how this methodology was able to optimize production through multi-attribute analysis by identifying anomalies within the seismic data. Another study by Roden and Chen (2017) showed how PCA and SOMs can better identify direct hydrocarbon indicator (DHI) characteristics. In another example, Chopra and Marfurt (2018) showed how unsupervised machine learning methods, such as PCA and SOMs, showed promising results in classifying seismic facies. By building off of these practical examples that use a multi-attribute machine learning approach to better characterize the subsurface, this study aims to use this methodology to improve our understanding of the constraints on the distribution of hydrates in the subsurface.

Principle component analysis (PCA)

PCA is a linear mathematical technique that reduces a set of variables, such as seismic attributes, to a set that illustrates the majority of uncorrelated information's variation (Jolliffe 2002; Sacrey and Roden 2014; Roden et al. 2015). The first principal component accounts for the most variability in the data with each succeeding orthogonal component accounting for the remaining variability. Although the first principal component highlights the largest linear attribute combinations that best represents the variability of the bulk of the data, it may not identify specific features that are of interest to the interpreter (Sacrey and Roden 2014; Roden et al. 2015). Therefore, succeeding principal components were evaluated because they may be associated with BSR characteristics not identified with the first principal component. When PCA is applied to a large set of seismic variables, such as seismic attributes, this will aid in identifying meaningful combinations of attributes that best reveal the discontinuous BSRs. Additionally, many attributes that are most likely to aid in locating the base of the GHSZ, such as attributes sensitive to the gas in the pore space or to acoustic impedance changes, were pre-selected to be used within the PCA.

Self-organizing maps (SOMs)

Following PCA analysis, the attributes deemed the most successful for revealing BSRs are then incorporated in a SOM. Due to the multidimensional nature of PCA results, SOMs are employed to help visualize these attribute relationships. A SOM is a collection of neurons that classify data samples into categories based on their various geological or geophysical properties. This is done by projecting the clusters onto a latent space for visualization (Kohonen 1990; Roy 2013). Several SOM hyperparameters were tested such as neuron count and the number of epochs (iterations). A detailed generalized schematic of the workflow is shown in Fig. 4.

Full- and angle- stack seismic data were used within the seismic attribute analysis. Several AVA attributes were calculated and evaluated, including those studied in Bedle (2019). However, gas indicator and Shuey's fluid factor were the two primary AVA attributes that stood out from PCA. Gas indicator is a logarithmic AVA attribute that has traditionally been used to highlight gas sands with a Class 2 AVA response. It is defined as the intercept multiplied by the natural log of the gradient's absolute value (Veeken 2007). Gas indicator ranked as the only attribute in the ninth eigenvector, effectively representing the entire eigenvector, and is thus recognized as unique variability in the dataset. Bedle (2019) suggests that gas indicator could be one of the better

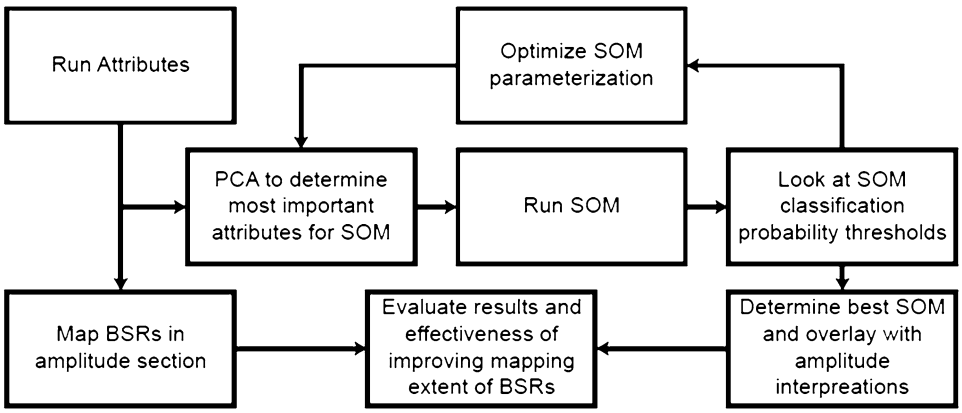

Fig. 4 Iterative SOM workflow used to evaluate the accuracy and effectiveness of each SOM result. Several combinations of instantaneous and AVA attributes as well as different neuron parameters were evaluated

attributes for highlighting Class 2 AVA responses. This was verified by the PCA through its use in the SOM analysis to better visualize weak BSRs. Shuey's fluid factor (Shuey 1985; Smith and Gidlow 2003) is another AVA attribute useful in highlighting Class 2 AVA sands and is calculated using the seismic intercept and gradient. Fluid factor consistently ranked at over 80% in eigenvector contribution for the first three eigenvectors, meaning that fluid factor is a good representation of the independent variability in the seismic dataset and could be helpful in revealing the hidden BSRs. Multiple instantaneous attributes were also evaluated with instantaneous frequency, sweetness, and thin bed consistently ranking at over 80% in eigenvector contribution in the first three eigenvectors.

There was also a balance to be struck between clustering every detail within the seismic that excluded noise while also optimizing the number of neurons to render the model computationally efficient. Several different combinations of neuron and epoch (iteration) counts were created to determine the optimal value. This is shown in Fig. 5a–f where we compare SOM models with different neuron and epoch counts. The first SOM model, shown in Fig. 5a, used an 8×8 neuron count with 100 epochs. This SOM parameterization was found to be computationally inefficient as it classified the same feature, such as high amplitude BSRs, in different clusters (shown in Fig. 5b). Furthermore, this model classified a significant amount of seismic noise within empty neurons (shown in Fig. 5c). Upon overlapping both the redundantly classified, high amplitude BSRs with the classified seismic noise (shown in Fig. 5d), it becomes apparent that the number of neurons should be reduced to optimize the model. The number of neurons was reduced down to 36 (shown in Fig. 5e) and was trained for 100 epochs. Notice how this model was able to achieve near identical results to those observed in Fig. 5a. Further analysis reduced the number of epochs down to 50 (shown in Fig. 5f) and also achieved similar results to Fig. 5a. This study found that a SOM model with 36 neurons and 50 epochs (shown in Fig. 5f) was able to achieve nearly identical results to a SOM model which used 64 neurons and 100 epochs (shown in Fig. 5a). However, SOM models that used less than 36 neurons returned results that did not detect as many of the weak BSR extents. Therefore, the optimized SOM model was run on a 6×6 neuron count (total of 36 neurons) with 50 epochs for both lines. These neuron dimensions and number of epochs were used because they are robust enough to highlight minute changes and details within the seismic data, such as the base of the GHSZ, while also being computationally efficient.

Results

After the number of neurons and epochs were optimized, this study then evaluated the number of attributes to use within the optimized model. The number and combination of attributes to use in a SOM model were determined using a combination of PCA and different SOM runs. These SOM results were compared to the far angle stack amplitude section of Line 19 from the PEG09 survey (Fig. 6a, b). One of the first SOM results (Fig. 6c, d) used an 8×8 matrix as well as eight instantaneous attributes. These instantaneous attributes included: envelope, envelope slope, Hilbert, instantaneous frequency, normalized amplitude, relative acoustic impedance, sweetness and thin bed (Fig. 6c, d). These attributes were chosen from PCA results and Table 1describes the definitions and uses of these attributes.

These eight attributes all ranked over 70% in eigenvector contribution within the first three eigenvectors for the initial SOM results. When these attributes were used in conjunction with each other, the base of the GHSZ was better imaged in the SOM results. However, similar to previous analyses in Fig. 5, several of the neurons were redundant and classified a significant amount of seismic noise. Also, several neurons needed to be displayed (shown in Fig. 6d) to generate the same result seen in Fig. 6e, f. Therefore, the model was computationally inefficient and was improved to achieve the same level of accuracy in a shorter time with less

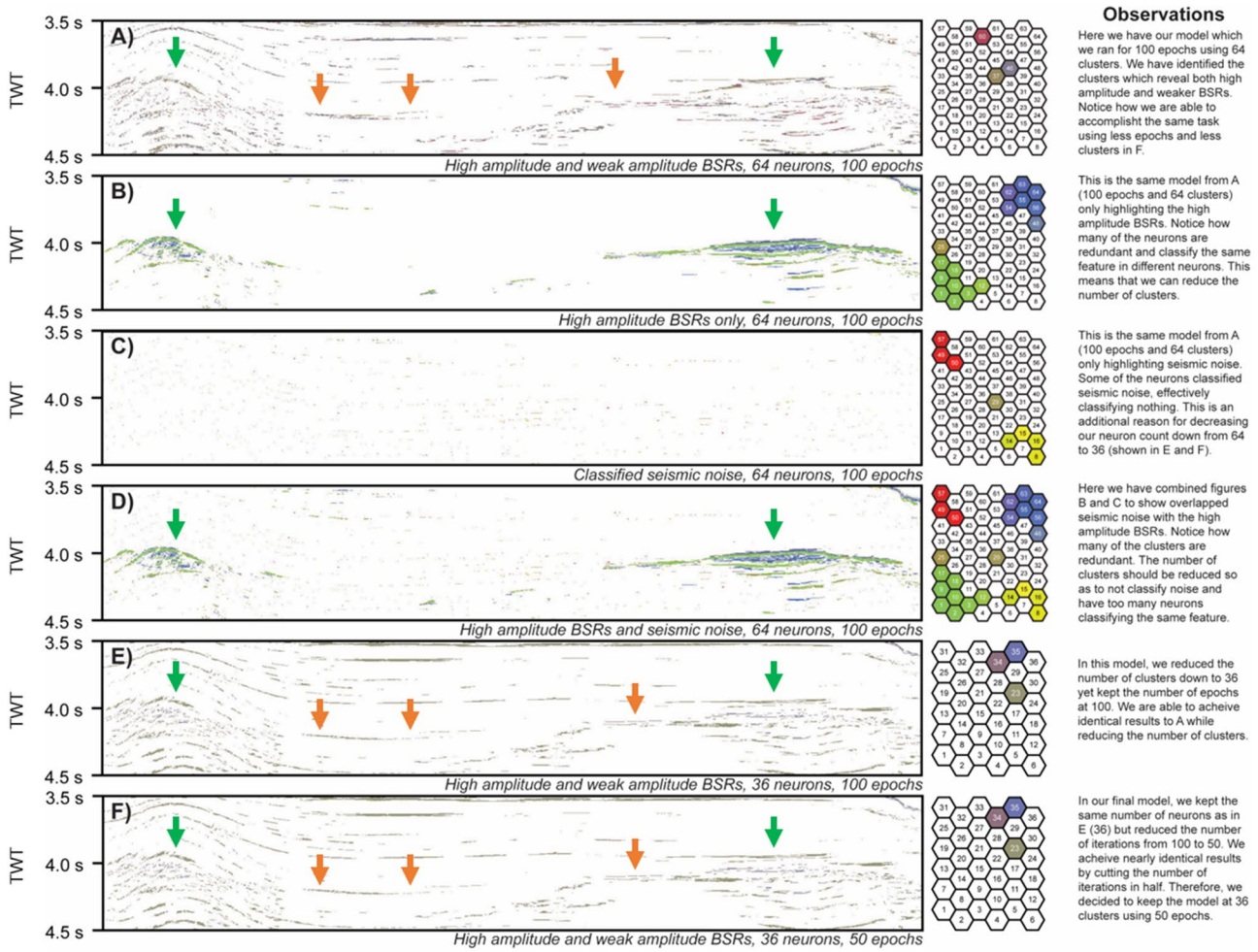

Fig. 5 Comparison of various SOM models with different epochs and neurons counts run on Line 19 of the PEG09 survey. **a** The model with 64 neurons trained for 100 epochs highlighting both strong and weak amplitude BSRs. **b** That same model with only the high amplitude BSRs whereas **c** shows the same model with only classified seismic noise highlighted. **d** The SOM model with 64 neurons trained for 100 epochs with classified high amplitude BSRs and seismic noise. Notice how many neurons redundantly classify the high amplitude BSRs and classify seismic noise. The neuron count was then reduced to 36 neurons in **e**. We then reduced the number of epochs down to 50 in **f** to obtain the same result as in **e**. This shows that by reducing the number of iterations and number of clusters, we are able to obtain the same results from model (**a**) in model (**f**) to achieve a more computationally efficient model. The green arrows represent high amplitude BSRs whereas the orange arrows represent the weak amplitude BSRs better revealed using our model

computational intensity. The optimized SOM ran with 36 neurons and five attributes: instantaneous frequency, sweetness, thin bed, fluid factor and gas indicator (Fig. 6e, f). Results found that the five attributes, which used a combination of both instantaneous and AVA attributes, were sufficient in improving the detection of weak BSRs. A larger number of attributes tended to render the algorithm computationally inefficient and any fewer tended to not include the furthest extent of the indistinct BSRs.

Once the best SOM parameters were determined for the PEG09 Line 19, this parameterization was then applied to the PEG09 survey with the raw, uninterpreted results of Line 6 and 19 shown in Fig. 7a. Once the raw SOMs neurons were interpreted, as shown in Fig. 7b, the results helped enhance the lateral extent of weak BSRs and how they are potentially connected to the high amplitude BSRs within the Pegasus Basin. The green arrows in Fig. 7b indicate the high amplitude BSRs whereas the orange arrows highlight the better detected weak BSRs within the seismic data. The SOM was able to resolve the previously hidden BSR, enhancing our understanding of the extent of hydrates within the PEG09 survey. After the SOM model was optimized for the PEG09 survey, an identical parametrization was applied to the APB13 survey to test if this gas hydrate detection method is transferable to other seismic surveys. The same SOM model and number of attributes were applied to the APB13 survey and the raw, uninterpreted and interpreted SOM results are displayed with Lines 17 and 38 as shown in

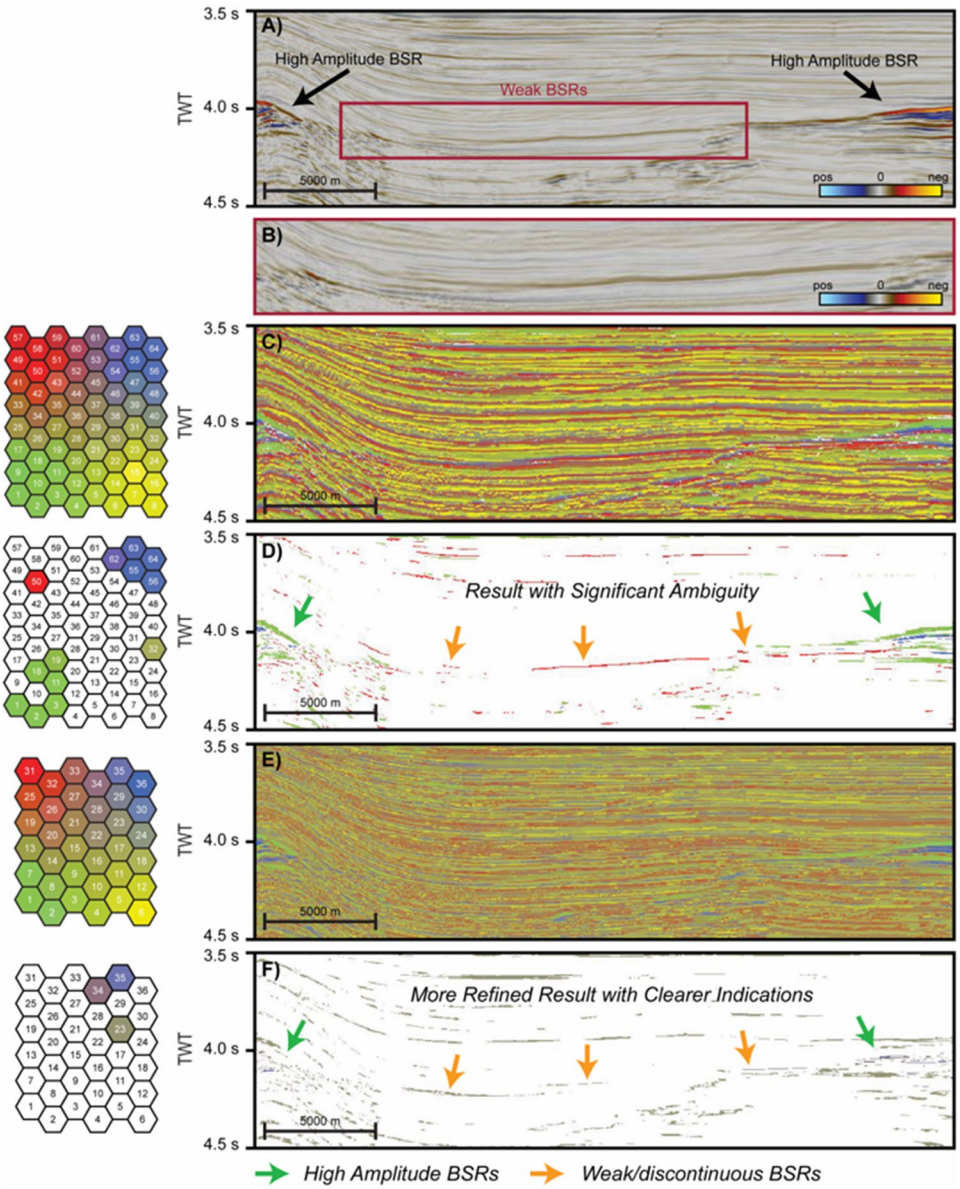

Fig. 6 Comparison of an unoptimized SOM result compared to an optimized SOM result. **a** PEG09 Line 19 amplitude section (refer to Fig. 2 for location relative to PEG09 2D survey) where weak, discontinuous BSRs are present between two areas of high amplitude BSRs. **b** A closer look at the weak BSR section highlighted in **a**. **c** The result from an optimized SOM with all of the neurons activated and displayed and **d** only shows the neurons which highlight the BSRs from **c**. Although the SOM helps highlight some of the weak BSRs, several similar neurons classified them and the calculation time could be significantly reduced. **e** Represents the SOM result with optimized parameters and all neurons displayed whereas **f** only shows the neurons which highlight the BSRs. With the SOM parameters optimized, similar results are achieved with a smaller number of neurons and computation time is significantly improved

Fig. 8a-b. Similar to the results from the PEG09 survey, the optimized SOM model was able to better resolve the weak BSRs within the APB13 survey that were previously hidden in the amplitude sections, shown by the orange arrows in Fig. 8b. It was also interesting to note that both surveys had the same specific neurons (23, 34 and 35) that classified the weak BSRs whereas the other neurons grouped different geologic features such as bedding, and other lithology variations. We interpret the orange arrows in both SOM results as weak BSRs because the clusters displayed from neurons 23, 34 and 35 are discontinuous and are heavily weighted towards Class 2n AVA attributes.

Neurons 23, 34 and 35 are most heavily weighted by a combination of fluid factor and far stack amplitude, fluid factor and instantaneous frequency, as well as far stack amplitude and instantaneous frequency. Overall, a combination of fluid factor and far stack amplitudes appears to be the most revealing for indistinct BSRs with a smaller influence in cluster weighting due to instantaneous frequency. AVA attributes such as fluid factor and gas indicator are helpful in identifying these weak BSRs as these attributes are particularly sensitive to the presence of gas within the pore space (Shuey 1985; Smith and Gidlow 2003; Veeken 2007). Instantaneous attributes such as instantaneous frequency, sweetness and thin bed indicator, are particularly helpful for analyzing bed thicknesses, identifying "sweet spots" in hydrocarbon exploration, and for locating the edges of low impedance thin beds (Taner et al. 1979; Hart 2008; Subrahmanyam and Rao 2008; Koson et al. 2014). These instantaneous attributes are especially helpful for better visualizing

Table 1 Definitions, uses and sources for all of the attributes presented within this study

Instantaneous attribute name	Definition	Uses	Sources
Hilbert	90-degree transform/rotation of the seismic trace complex trace	These attributes are useful to highlight discontinuities such as faults or lithology changes (Taner et al. 1979; Chopra and Marfurt 2005). These attributes are also helpful for analyzing AVA anomalies as both attributes are proportional to reflectivity (Taner et al. 1979; Subrahmanyam and Rao 2008)	Taner et al. (1979), Chopra and Marfurt (2005), Subrahmanyam and Rao (2008)
Envelope	Calculated from the complex trace to highlight the signal's instantaneous energy		
Envelope Slope	Calculated from the complex trace to highlight the signal's change in reflectivity		
Instantaneous Frequency	Calculated by taking the time derivative of phase	This attribute is beneficial for analyzing bed thicknesses and for indicating the edges of low impedance thin beds, such as in the case of weak BSRs (Taner et al. 1979; Subrahmanyam and Rao 2008)	Taner et al. (1979), Subrahmanyam and Rao (2008)
Sweetness	Computed by dividing the envelope by the square root of instantaneous frequency	First discovered by Radovich and Oliveros (1998), sweetness is a relative value helpful for determining relative net-to-gross ratios and to identify "sweet spots" in hydrocarbon exploration (Hart 2008; Koson et al. 2014)	Radovich and Oliveros (1998), Hart (2008), Koson et al. (2014)
Thin Bed (also known as thin bed indicator)	Calculated by subtracting the derivative of instantaneous frequency from instantaneous frequency. This is achieved by extracting the location of where instantaneous frequencies change directions or become negative within the seismic data (Taner 2001). Taner (2001) attributes these sign reversals resulting from wavelets arriving close to one another	Large variations of instantaneous frequency will help identify the location of these thin beds and highlight them within the seismic response (Taner 2001; Subrahmanyam et al. 2008)	Taner (2001); Subrahmanyam and Rao (2008)
AVA attribute name	**Definition**	**Uses**	**Sources**
Gas indicator	Calculated by multiplying the intercept by the natural log of the gradient's absolute value	This attribute has been traditionally used to highlight gas sands with a Class 2 AVA response	Veeken (2007)
Shuey's fluid factor	Calculated from using the intercept and the gradient	Another AVA atrtibute that is useful for highlighting Class 2 AVA sands	Shuey (1985), Smith and Gidlow (2003)

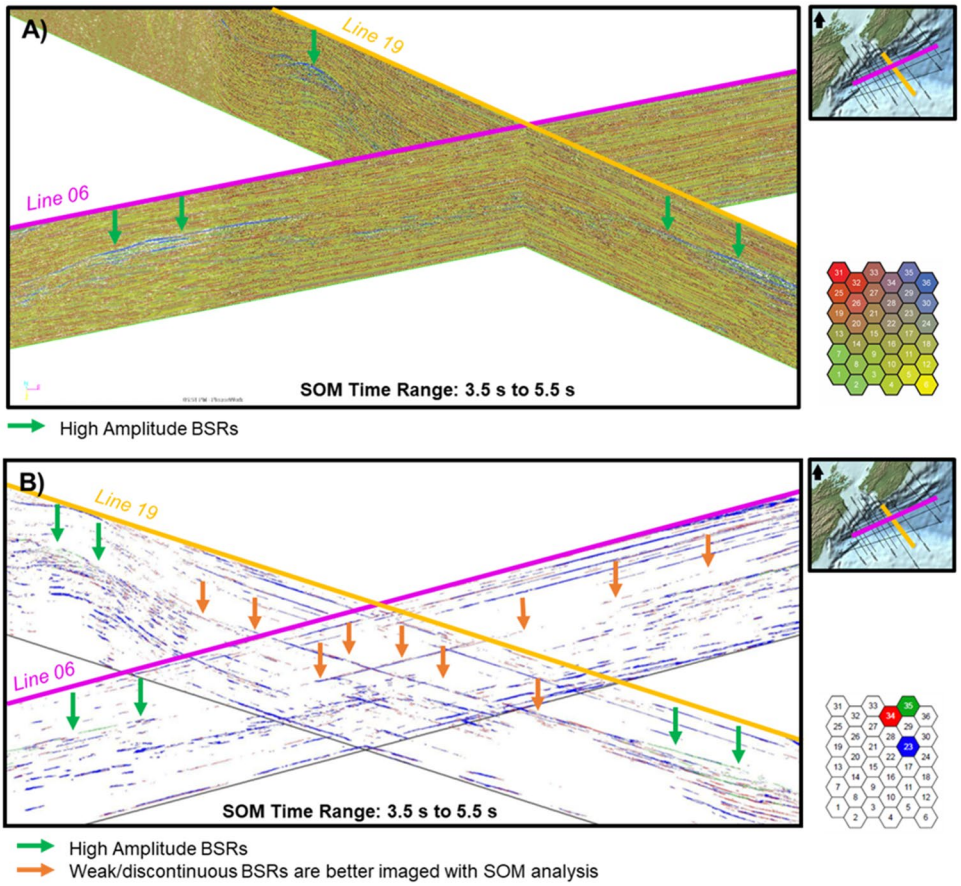

Fig. 7 **a** Raw SOM results for Lines 06 and 19 within the PEG09 2D seismic survey and **b** optimized SOM results for Lines 06 and 19 within the PEG09 2D seismic survey revealing the better imaged BSR

weak BSRs that have low impedance contrasts due to their slight increase in amplitude as a result of hydrates within the pore space (Spence et al. 2010; Lui and Lui 2018). Rather than using seismic attributes separately to identify BSRs with limited resolution, the SOM improves the imaging and understanding of gas hydrate presence by combining several seismic attributes. BSRs are better identified when using a multi-attribute analysis that complements AVA attributes sensitive to the presence of gas in the pore space with other instantaneous attributes highlighting bed thicknesses and low impedance contrasts.

PCA results for both surveys showed near identical eigenvalues across the different eigenvectors (Fig. 9). Here, the "% Max" represents that same attribute variance displayed as a percentage of the largest eigenvector whereas "Percentage" represents how much each attribute contributed toward that eigenvalue. Attributes are ranked in similar orders throughout all of the eigenvectors for both surveys (shown by the black arrows in Fig. 9). Additionally, the eigenvalues from both surveys are nearly identical, demonstrating that the data clusters within the seismic surveys are also quite similar.

Notice how the maximum percentage contribution of the attributes rank in similar order with similar values for eigenvalue 2 (shown by the red arrows in Fig. 9). For the PEG09 survey, these two attributes (instantaneous frequency and thin bed) contributed approximately 33% to eigenvector 2 and represented a significant amount of the variance for the PEG09 dataset (shown under % Max in Fig. 9). This same relationship for eigenvector 2 in the PEG09 survey was also observed for the APB13 survey. Attributes such as instantaneous frequency and thin bed also shared similar percentage and percent max values. For this reason, these attributes were used in the final SOM model as they contributed a significant amount to the first few eigenvectors and represented the majority of the variance from each dataset (highlighted in green in Fig. 9). These relationships illustrate that these attributes reveal identical distributions with the seismic data and that this method is transferable to other areas. SOM clusters were identical in both the PEG09 and APB13 surveys and successfully detected weak BSRs that were previously hidden within the seismic data. These results detected previously unknown gas hydrate accumulations where BSRs are indistinct, clearly showing that there are gas hydrate accumulations throughout the basin and not just where the high amplitude BSRs are observed.

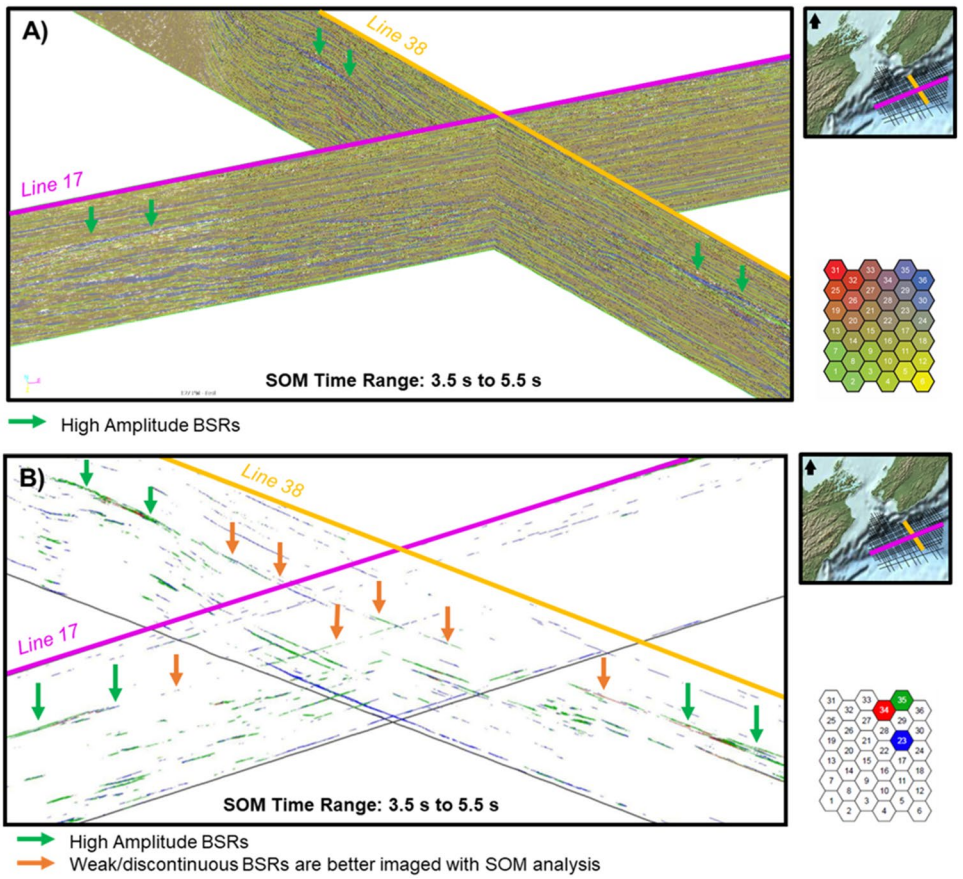

Fig. 8 **a** Raw SOM results for Lines 17 and 38 within the APB13 2D seismic survey and **b** optimized SOM results for Lines 17 and 38 within the APB13 2D seismic survey revealing the better imaged BSR

PEG09 Survey

Eigenvector for Selected Eigenvalue: 2

Attribute Name	Percentage	% Max
PEG09 Instantaneous Frequency	30.50	81.37
PEG09 Thin Bed	29.91	79.79
PEG09 Acceleration of Phase	18.86	50.31
PEG09 Envelope Second Derivative	3.86	10.31
PEG09 Original Amplitude Data	3.80	10.14
PEG09 Envelope Slope	3.55	9.48
PEG09 Fluid Factor	3.45	9.20
PEG09 Normalized Amplitude	2.34	6.23

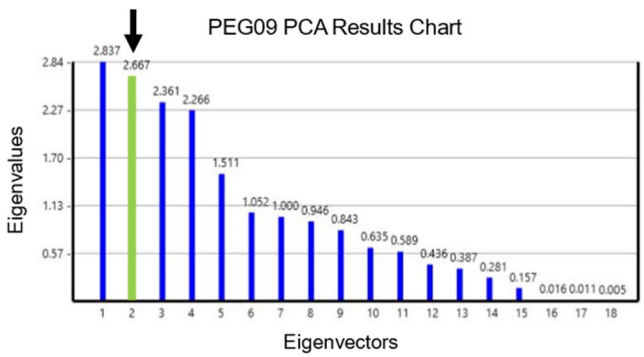

APB13 Survey

Eigenvector for Selected Eigenvalue: 2

Attribute Name	Percentage	% Max
ABP13 Instantaneous Frequency	34.23	91.90
ABP13 Thin Bed	33.71	90.51
ABP13 Acceleration of Phase	22.52	60.46
ABP13 Envelope Second Derivative	4.22	11.33
ABP13 Envelope Slope	2.45	6.58
ABP13 Smoothed Frequency	1.94	5.20
ABP13 Bandwidth	0.24	0.65
ABP13 Envelope	0.15	0.41

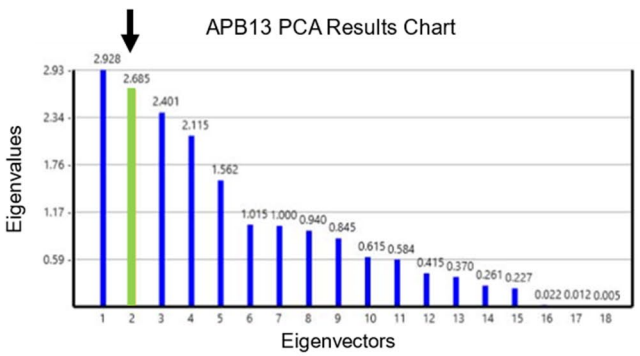

Fig. 9 Comparison of the PCA results between the PEG09 and APB13 2D seismic surveys showing the evident similarity between them. Attributes are ranked in very similar orders within all eigenvectors with similar eigenvalues (shown by the black and red arrows). These results, along with the similar SOM results, show that this methodology is transferrable

Discussion

The amplitude response strength of BSRs is related to the amount of trapped free gas beneath them (Henrys et al. 2009). There are still significant ongoing studies into better understanding the source of gas and its migration into the GHSZ (Kroeger et al. 2015, 2019). Xu and Ruppel (1999) illustrated how gas migrates upwards in solution along permeable fault pathways until it reaches the base of the GHSZ, where gas concentration surpasses solubility. This transition from gas in solution to free gas causes a sudden increase in velocity, or seismic impedance, thus creating the observed high-amplitude BSRs in the Pegasus Basin. This migration concept is further supported by Plaza-Faverola et al. (2012) where they investigated the accumulation and distribution of concentrated hydrate zones as a result of focused fluid flow within the basin. Many of the migration pathways for gas hydrates originated from gas chimneys that are related to underlying faults. These fluids can migrate vertically towards topographic highs, such as towards the frontal anticline, or towards traps, such as the triangular trap formed by the dipping Chatham Rise and other hydrate bearing sediments (Plaza-Faverola et al. 2012; Crutchley et al. 2019; Turko et al. 2020). This pattern is well observed in Fig. 10 where the high amplitude BSRs overlap with structural elements in the study area and further illustrate the migration pathways for gas within the Pegasus Basin. This is further supported from significant attenuation observed along these migration pathways where free gas is present (shown in Figs. 3a–d and 10). Additionally, gas was sampled at vent sites on the seafloor and revealed that the gas also had microbial origin (Kroeger et al. 2015).

However, in regions where strata are laterally continuous with no significant dip, it is difficult for free gas to become trapped and create high-amplitude BSRs. This inability for free gas to become trapped below hydrate-bearing sediment in a flat lying sediment layer within a package of flat lying sediments that have relatively uniform lithology will create an amplitude response that is difficult to discern from other reflectors indicative of background geology. If neurons 23, 34 and 35 were to represent lithology in Figs. 7a, b and 8a, b, the clusters would be laterally continuous in time and well defined across the survey. This assumption is only valid where lithology does not vary laterally and may not hold near the Hikurangi Channel in the Pegasus Basin where there are several phases of Pleistocene channel/levee complexes (Kroeger et al. 2019). However, the theoretical seismic response will be different for hydrate-bearing and non-hydrate-bearing sediments as the inclusion of hydrate in the pore space for a brine case would produce a weak Class 2n AVA response (Bedle 2019). By using this study's proposed multi attribute machine learning model, hydrate bearing sediments were able to be differentiated from non-hydrate bearing sediments at the base of the GHSZ. This differentiation is well highlighted in Figs. 7 and 8 where we were able to infer where other hydrate-bearing sediments may be located where there is no significant geologic dip. The location of these features is also in accordance with the expected temperature and pressure conditions for gas hydrates to exist within the Pegasus Basin (Plaza-Faverola et al. 2012; Kroeger et al. 2015).

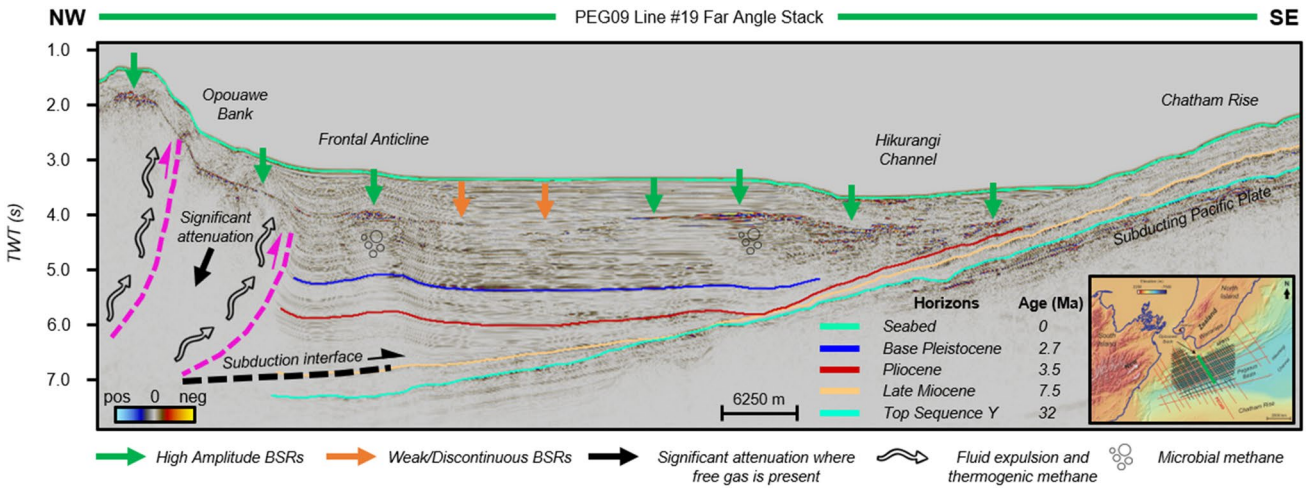

Fig. 10 Structural and stratigraphic interpretation of Line 19 from the PEG09 survey highlighting the various migration routes for gas within the Pegasus Basin. Horizons and faults were modified from Kroeger et al. (2015) and interpreted on a time volume. Fluid expulsion, thermogenic methane pathways and microbial methane modified after Henrys et al. (2009), Plaza-Faverola et al. (2012) and Kroeger et al. (2015). Bathymetry map taken from the General Bathymetric Chart of the Oceans (GEBCO) Compilation Group (2019)

While seismic attributes on their own have limited success in identifying weak BSRs, combining attributes together helped to better characterize and visualize these often seismically transparent hydrate accumulations. SOM models that only combined instantaneous attributes were successful in teasing out some of the weak BSRs but were further improved once incorporated with AVA attributes such as fluid factor and gas indicator. Figure 11a–g displays the individual attributes that were used for the final SOM. The final SOM result (Fig. 11a) is shown alongside the far angle stack of Line 19 from the PEG 09 survey (Fig. 11b). Instantaneous frequency in Fig. 11c and gas indicator in Fig. 11f seemed to highlight the other subtle responses related to the weak and discontinuous BSRs. Attributes such as thin bed in Fig. 11d and sweetness in Fig. 11e seem to help image some of the weaker BSRs and further compliment the other attribute results. The fluid factor attribute in Fig. 11g matched nearly exactly with the SOM results in Fig. 11a. These observations are in accordance with the previously discussed cluster analysis where the three neurons (23, 34 and 35) were most heavily weighted by a combination of fluid factor in combination with far stack amplitude and instantaneous

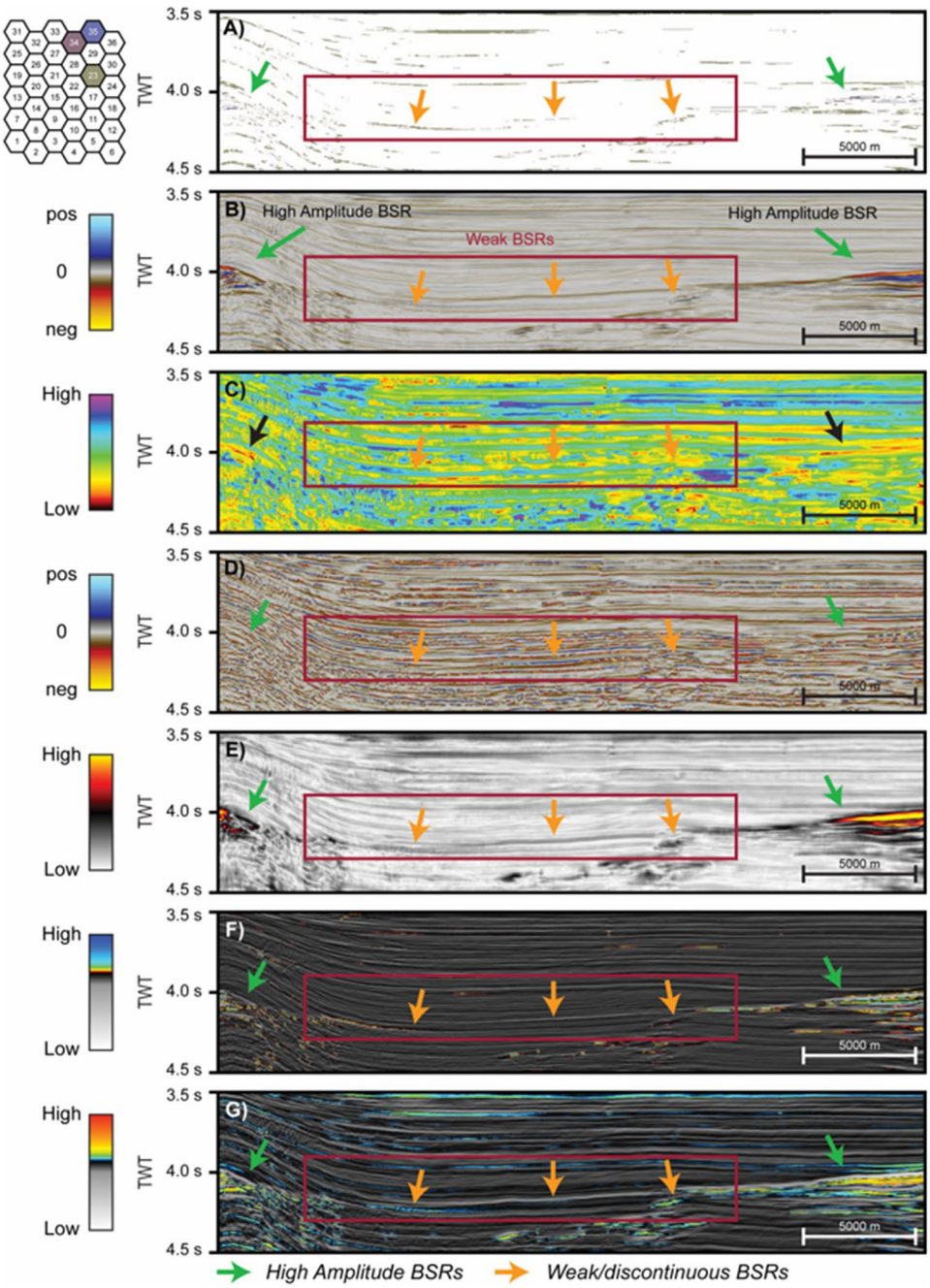

Fig. 11 **a** Optimized SOM results (from Fig. 6f) for Line 19 of the PEG09 2D survey shown relative to the **b** far angle stack amplitude section for Line 19 and all of the seismic attributes used within the SOM: **c** instantaneous frequency, **d** thin bed, **e** sweetness, **f** gas indicator, **g** shuey fluid factor seismic attributes. It appears that the fluid factor attribute contributed the most towards the SOM result. This is later confirmed by weighted contribution analysis for neurons 23, 34 and 35. Additionally, attributes such as sweetness and AVA attributes were able to detect high amplitude BSR response quite well

frequency. These neurons also had minor contributions from other attributes such as gas indicator, thin bed and sweetness which could be further complimenting the more dominant attributes to further reveal the extent of hydrates in the subsurface. Also, these results indicate that there is a Class 2n AVA response for hydrate presence in a brine case while also highlighting the Class 3 AVA responses for hydrates with trapped free gas beneath them. Therefore, AVA attributes such as gas indicator and fluid factor are helpful in highlighting these features. However, instantaneous frequency still had a significant percentage contribution within each of the neurons. Therefore, both weak and strong amplitude BSRs are better identified when using other instantaneous attributes that are helpful in highlighting bed thicknesses and low impedance contrasts, which in turn complements AVA attributes that are sensitive to the presence of gas in the pore space. Figure 12 illustrates the enhanced interpretation capabilities for hydrates in the PEG09 and APB13 survey using the proposed SOM workflow.

Additionally, all of the attributes used in the final SOM were able to detect and image the high amplitude BSRs within neurons 23, 34 and 35. Figure 13a–d shows these SOM clusters highlighting the high amplitude BSRs and enhancing their interpretability on Line 30 of the APB13 survey. However, these high amplitude BSR clusters only represented a small percentage of the classified data points within those neurons meaning that the displayed neurons primarily identified anomalous weak BSRs. Similar observations were also noted for the APB13 survey SOM result. Figure 14a–d shows how the some of these weaker BSRs are better highlighted using our proposed SOM model and their enhanced interpretability on Line 30 of the APB13 survey. The neurons also exhibited higher weighting towards fluid factor in combination with gas indicator and instantaneous frequency. This higher weighting towards attributes such as gas indicator and fluid factor could be due to how successful they are in identifying the presence of gas and other anomalous fluids within the pore space by revealing Class 2 and 3 AVA anomalies. There may have also been a higher weight towards instantaneous frequency as this attribute is helpful for indicating the edges of low impedance thin beds, such as is the case for weak BSRs (Taner et al. 1979; Subrahmanyam and Rao 2008). A study conducted by Navalpakam et al. (2012) along the Hikurangi Margin found that weak BSRs are primarily caused by low gas saturation where gas is only present within pores or fractures with a patchy distribution. Therefore, attributes such as fluid factor and gas indicator are prime candidates for identifying this patchy gas saturation and further revealing weak BSRs in our study area. The results also helped to detect weak BSRs over the same study area, however, in a different survey. This is because PCA analysis revealed that the PEG09 and APB13 surveys were nearly identical with attributes ranking in the same order in different eigenvectors.

The PCA and SOM results show that the model is applicable to different seismic surveys and can help resolve weak BSRs. Another interesting observation was that SOM result for Line 17 of the APB13 survey detected no weak BSRs in the eastern portion when it did detect these in the PEG09 survey. This is hypothesized to be due to two primary

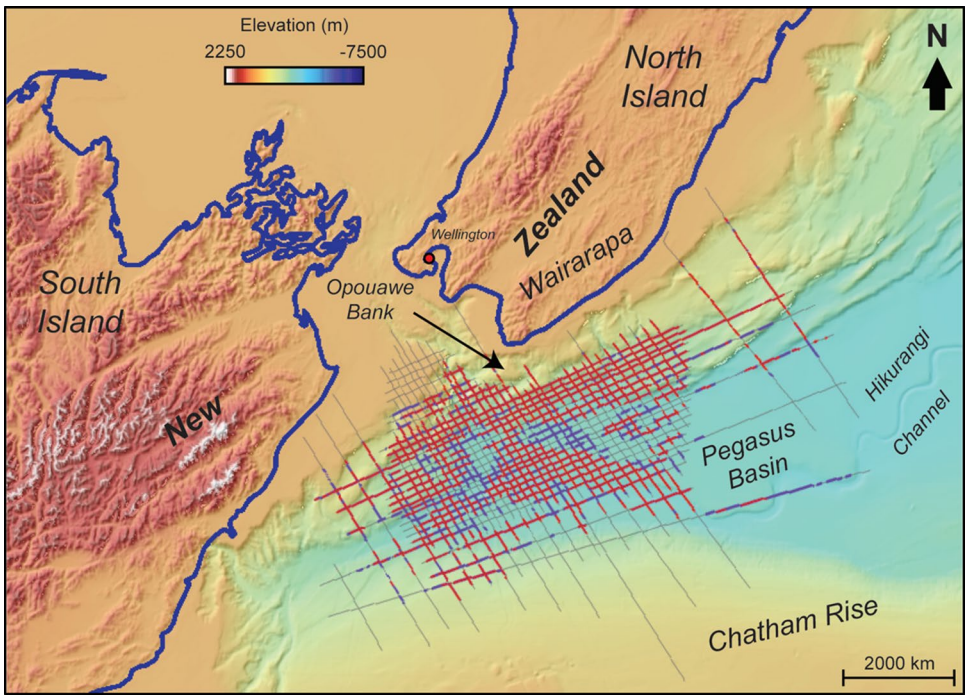

Fig. 12 Enhanced BSR interpretation capabilities for hydrates in the both the PEG09 and APB13 survey (grey lines) using the proposed SOM. Individual amplitude and seismic attribute interpretations are shown in red whereas the improved interpretation using our proposed SOM model is shown in purple. Bathymetry map taken from the General Bathymetric Chart of the Oceans (GEBCO) Compilation Group (2019)

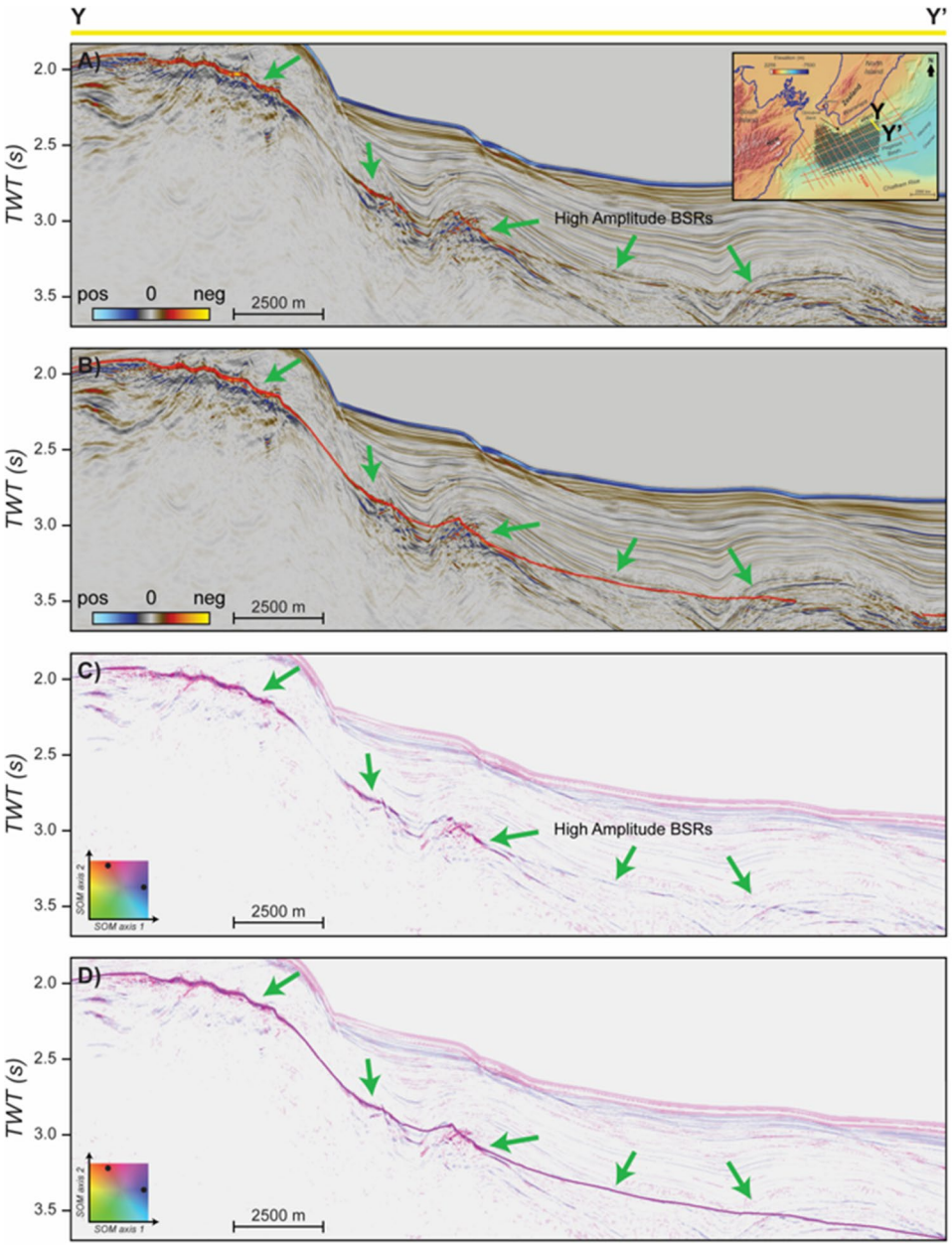

Fig. 13 **a** Far angle stack Line 62 from the APB13 survey with **b** the interpreted BSRs (in red) whereas **c** shows the SOM results from another software and **d** the enhanced interpretability (in purple) as a result of the proposed SOM model. The green arrows are pointing to high amplitude BSRs. Bathymetry map taken from the General Bathymetric Chart of the Oceans (GEBCO) Compilation Group (2019)

reasons. The first being that these lines are slightly offset from one another as the 2D lines belong to separate surveys. The distance between the PEG09 and APB13 survey lines is approximately 3500 m, which could be enough for the weak BSR from Line 06 in the PEG09 survey to fade. Another reason is that there appears to be no minor anomalies within the seismic amplitude and attributes. When looking closer at the fluid factor attribute over the eastern portion of Line 17 from the APB13 survey, there were no anomalies observed from Line 06 of the PEG09 survey. Therefore, it is hypothesized that the SOM for APB13 did not map the missing weak BSR as there most likely was no weak BSRs in that region. If there were no observed Class 2n AVA anomalies, it is possible that there are no hydrates present in the pore space. This could be due to the fact that there is not a homogeneous generation of methane throughout the entire Pegasus Basin (based on the models presented in Plaza-Faverola et al. 2012; Kroeger et al. 2015, 2019). Additionally, it could be that the migration pathways feeding other or older populations of methane into the area do not exist for some structural or geologic reason. Hydrate accumulations near structural highs are primarily controlled by fluid focusing and transport of methane (Henrys et al. 2009; Plaza-Faverola et al. 2012; Crutchley et al. 2019). However, in areas where the generation and/or migration of microbial methane are not present, no gas hydrates can form.

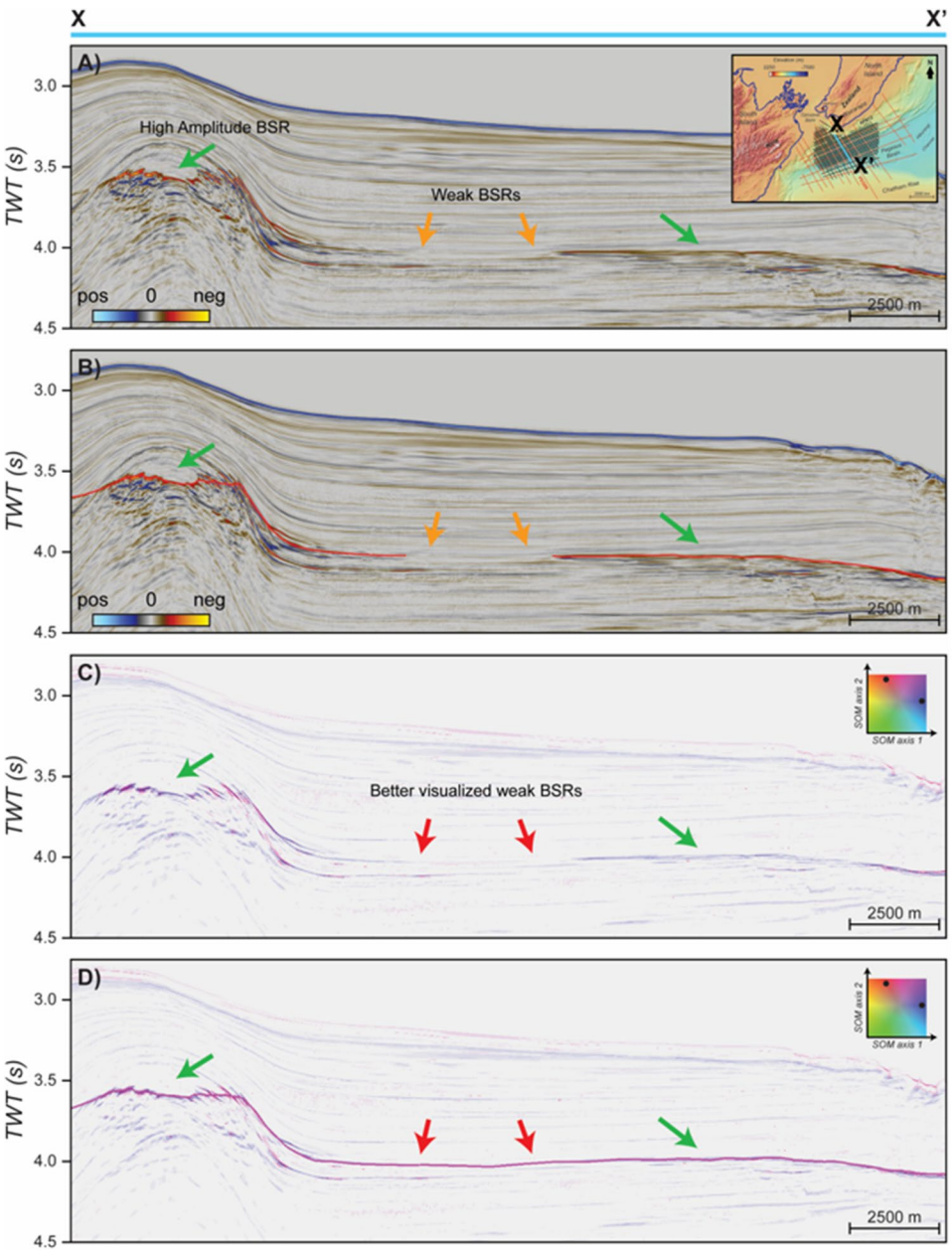

Fig. 14 **a** Far angle stack Line 30 from the APB13 survey with **b** the interpreted BSRs (in red) whereas **c** shows the SOM results from another software and **d** the enhanced interpretability (in purple) as a result of the proposed SOM model. The green arrows are pointing to high amplitude BSRs, the orange arrows are pointing to the weak amplitude BSRs and the red arrows are pointing to the improved imaging of the weak amplitude BSRs using the SOM model. Bathymetry map taken from the General Bathymetric Chart of the Oceans (GEBCO) Compilation Group (2019)

A prominent diagnostic feature of hydrate-bearing sediments is an increase in both the P- and S-wave velocities once hydrate saturation exceeds approximately 40% (Dai et al. 2004, 2008a, b; Yun et al. 2007; Waite et al. 2009). There exists a wide range of models that are based on the amount of hydrate and the growth between hydrate and the sediment (Dai et al. 2004; Xu et al. 2004; Waite et al. 2009; Zhang et al. 2020). However, these models exhibit a wide range of elastic properties for hydrate-bearing sediments (Dai et al. 2004; Waite et al. 2009). Overall, these models nevertheless demonstrate that even a small amount of hydrate present within the sediments will create an increase in acoustic velocities (Dai et al. 2004; Waite et al. 2009). It is important to note that these models only account for the elastic properties and do not account for inelastic parameters such as attenuation (Dai et al. 2008a). Therefore, it may be difficult to resolve very small hydrate accumulations in the subsurface by only using the seismic amplitude response. This could be circumvented by reprocessing the data to highlight and preserve the amplitude of shallow geologic features to better visualize BSRs (Dai et al. 2004, 2008a). Finally, it is also important to note that there were other neurons that only identified high amplitude BSRs. However, this study is focused on better identifying weaker, less obvious BSRs that may be hidden within the seismic volume. These neurons could be beneficial for quick mapping and analysis of

prominent BSRs within a given area when using attributes which are sensitive to the inclusion of gas and help identify thin beds as well as low impedance contrasts.

Conclusions

Instantaneous attributes that detect changes in the frequency and phase of seismic data tend to cluster together in the PCA to reveal the interface at the base of the GHSZ. The extent and resolution of discontinuous BSRs from preliminary results are significantly improved when AVA attributes, such as gas indicator and fluid factor, were used in combination with instantaneous attributes sensitive to frequency, and small amplitude anomalies. Both weak and strong BSRs are better identified when using instantaneous attributes such as instantaneous frequency, sweetness and thin bed, which compliment AVA attributes such as gas indicator and fluid factor. Individually, some of these attributes have minimal success in identifying the seismically transparent hydrates. However, employing a multi-attribute analysis provides clearer insight and confidence into the identification and distribution of gas hydrates. PCA results for both the PEG09 and APB13 surveys were nearly identical demonstrating that this method for detecting gas hydrates is transferable to other surveys.

Acknowledgements We would like to acknowledge New Zealand Petroleum and Minerals for access to the Pegasus Basin 2D seismic surveys. Thank you to Geophysical Insights and Schlumberger for software license donations to the University of Oklahoma. We would also like to thank the General Bathymetric Chart of the Oceans (GEBCO) Compilation Group for the bathymetric data used in this study. An additional thank you to all of the University of Oklahoma faculty and students as well as the AASPI Consortium for their help and guidance throughout this project. Finally, we would like to thank the anonymous reviewers for the valuable feedback and recommendations for improving this manuscript.

Author contributions All authors contributed to the study conception and design. Material preparation, data collection and analysis were performed by JC and further verified by HB. HB provided much appreciated guidance and recommendations throughout this project. The first draft of the manuscript was written by JC and all authors commented on previous versions of the manuscript. All authors read and approved the final manuscript.

Funding This research was funded by initial startup funds from the University of Oklahoma.

Data availability We would like to thank New Zealand Petroleum and Minerals for open access to the Pegasus Basin 2D PEG and APB seismic surveys.Code availability This study used several different applications. We thank Geophysical Insights for providing their Paradise software package, the University of Oklahoma for providing the AASPI software package and Schlumberger for providing Petrel licenses. The authors used Paradise and AASPI for their machine learning analysis and used Petrel for seismic data interpretation.

Compliance with ethical standards

Conflict of interest The authors declare that they have no conflict of interest.

References

Anardarko New Zealand Ltd (2014a) Seismic data processing report—APB-13–2D Pegasus Basin 2D PEP54858. NZP&M, Ministry of Business, Innovation & Employment (MBIE). New Zealand unpublished petroleum report PR5171

Anardarko New Zealand Ltd (2014b) APB-13–2D Pegasus Basin 2D quality assurance report PEP 54861 marine 2D seismic survey PEP 54858. NZP&M, Ministry of Business, Innovation & Employment (MBIE), New Zealand unpublished petroleum report PR5172

Bedle H (2019) Seismic attribute enhancement of weak and discontinuous gas hydrate bottom-simulating reflectors in the Pegasus Basin, New Zealand. Interpretation 7(3):SG11–SG22

Bland KJ, Uruski CI, Isaac MJ (2015) Pegasus Basin, eastern New Zealand: a stratigraphic record of subsidence and subduction, ancient and modern. NZ J Geol Geophys 58(4):319–343

Chopra S, Castagna JP (2014) AVO. Soc Explor Geophys. https://doi.org/10.1190/1.9781560803201

Chopra S, Marfurt KJ (2005) Seismic attributes—a historical perspective. Geophysics 70(5):3–28

Chopra S, Marfurt KJ (2018) Seismic facies classification using some unsupervised machine-learning methods. SEG Tech Prog Expand Abstr 2018:2056–2060

Crutchley GJ, Kroeger KF, Pecher IA, Gorman AR (2019) How tectonic folding influences gas hydrate formation: New Zealand's Hikurangi subduction margin. Geology 47(1):39–42

Dai J, Xu H, Snyder F, Dutta N (2004) Detection and estimation of gas hydrates using rock physics and seismic inversion: Examples from the northern deepwater Gulf of Mexico. Lead Edge 23(1):60–66

Dai J, Snyder F, Gillespie D, Koesoemadinata A, Dutta N (2008a) Exploration for gas hydrates in the deepwater, northern Gulf of Mexico: Part I. A seismic approach based on geologic model, inversion, and rock physics principles. Mar Petrol Geol 25(9):830–844

Dai J, Banik N, Gillespie D, Dutta N (2008b) Exploration for gas hydrates in the deepwater, northern Gulf of Mexico: Part II. Model validation by drilling. Mar Petrol Geol 25(9):845–859

Dewangan P, Mandal R, Jaiswal P, Ramprasad T, Sriram G (2014) Estimation of seismic attenuation of gas hydrate bearing sediments from multi-channel seismic data: a case study from Krishna-Godavari offshore basin. Mar Pet Geol 58:356–367

Dvorkin J, Nur A (1996) Elasticity of high-porosity sandstones: theory for two North Sea data sets. Geophysics 61(5):1363–1370

Dvorkin J, Prasad M, Sakai A, Lavoie D (1999) Elasticity of marine sediments: rock physics modeling. Geophys Res Lett 26(12):1781–1784

Dvorkin J, Nur A, Uden R, Taner T (2003) Rock physics of a gas hydrate reservoir. Lead Edge 22(9):842–847
Ecker C, Dvorkin J, Nur AM (2000) Estimating the amount of gas hydrate and free gas from marine seismic data. Geophysics 65(2):565–573
Englezos P (1993) Clathrate hydrates. Ind Eng Chem Res 32(7):1251–1274
Faure K, Greinert J, Pecher IA, Graham IJ, Massoth GJ, De Ronde CE, Wright IC, Baker ET, Olson EJ (2009) Methane seepage and its relation to slumping and gas hydrate at the Hikurangi margin, New Zealand. NZ J Geol Geophys 49(4):503–516
Field ME, Barber JHJ (1993) A submarine landslide associated with shallow seafloor gas and gas hydrates off Northern California. Submarine landslides: selected studies in the US exclusive economic zone. US Geol Surv 2002:151–157
Finley PD, Krason J (1988) Geological evolution and analysis of confirmed or suspected gas hydrate localities No DOE/MC/21181-1950, vol 12. Geoexplorers International, Inc., Denver
GEBCO Compilation Group (2019) GEBCO 2019 grid.
Griffin AG, Bland KJ, Field B, Strogen DP, Crutchley G, Lawrence MJ, Kellett R (2015) Reservoir characterization of the East Coast and Pegasus basins, Eastern North Island, New Zealand. AAPG and SEG International Conference and Exhibition, Melbourne
Guerin G, Goldberg D, Meltser A (1999) Characterization of in situ elastic properties of gas hydrate-bearing sediments on the Blake Ridge. J Geophys Res Solid Earth 104(B8):17781–17795
Haacke RR, Westbrook GK, Hyndman RD (2007) Gas hydrate, fluid flow and free gas: formation of the bottom-simulating reflector. Earth Planet Sci Lett 261(3–4):407–420
Hart BS (2008) Channel detection in 3-D seismic data using sweetness. AAPG Bull 92(6):733–742
He L, Matsubayashi O, Lei X (2006) Methane hydrate accumulation model for the Central Nankai accretionary prism. Mar Geol 227(3–4):201–214
Henrys SA, Woodward DJ, Pecher IA (2009) Variation of bottom-simulating-reflection strength in a high-flux methane province, Hikurangi margin, New Zealand. AAPG Memoir 89:481–489
Hillman JI, Cook AE, Sawyer DE, Küçük HM, Goldberg DS (2017) The character and amplitude of 'discontinuous' bottom-simulating reflections in marine seismic data. Earth Planet Sci Lett 459:157–169
Holbrook SW, Hoskins H, Wood WT, Stephen RA, Lizarralde D (1996) Methane hydrate and free gas on the Blake Ridge from vertical seismic profiling. Science 273(5283):1840–1843
Jolliffe IT (2002) Mathematical and statistical properties of population principal components. In: Jolliffe IT (ed) Principal component analysis, 2nd edn. Springer, New York, pp 10–28
Katz HR (1981) Probable gas hydrate in continental slope east of the North Island, New Zealand. J Pet Geol 3(3):315–324
Katz HR (1982) Evidence of gas hydrates beneath the continental slope, East Coast, North Island, New Zealand. NZ J Geol Geophys 25(2):193–199
Kim HS, Cho GC, Lee JY, Kim SJ (2013) Geotechnical and geophysical properties of deep marine fine-grained sediments recovered during the second Ulleung Basin Gas Hydrate expedition, East Sea, Korea. Mar Pet Geol 47:56–65
Kohonen T (1990) The self-organizing map. Proc IEEE 78(9):1464–1480
Koson S, Chenrai P, Choowong M (2014) Seismic attributes and their applications in seismic geomorphology. Bull Earth Sci Thail 6(1):1–9
Kroeger FK, Plaza-Faverola A, Barnes PM, Pecher IA (2015) Thermal evolution of the New Zealand Hikurangi subduction margin: impact on natural gas generation and methane hydrate formation—a model study. Mar Pet Geol 63:97–114
Kroeger KF, Crutchley GJ, Kellett R, Barnes PM (2019) A 3D model of gas generation, migration and gas hydrate formation at a young convergent margin (Hikurangi Margin, New Zealand). Geochem Geophys Geosyst. https://doi.org/10.1029/2019GC008275
Lewis KB, Collot JY, Lallem SE (1998) The dammed Hikurangi Trough: a channel-fed trench blocked by subducting seamounts and their wake avalanches (New Zealand-France GeodyNZ Project). Basin Res 10(4):441–468
Liu T, Liu X (2018) Identification of morphologies of gas hydrate distribution based on amplitude variation with angle analysis. Geophysics 83(3):B143–B154
Makogon YF, Holditch SA, Makogon TY (2007) Natural gas-hydrates—a potential energy source for the 21st Century. J Petrol Sci Eng 56(1–3):14–31
Navalpakam RS, Pecher IA, Stern T (2012) Weak and segmented bottom simulating reflections on the Hikurangi Margin, New Zealand—implications for gas hydrate reservoir rocks. J Petrol Sci Eng 88:29–40
Nimblett J, Ruppel CD (2003) Permeability evolution during the formation of gas hydrates in marine sediments. J Geophys Res Solid Earth 108:B9
Plaza-Faverola A, Klaeschen D, Barnes P, Pecher I, Henrys S, Mountjoy J (2012) Evolution of fluid expulsion and concentrated hydrate zones across the southern Hikurangi subduction margin, New Zealand: an analysis from depth migrated seismic data. Geochem Geophys Geosyst 13:8
Radovich BJ, Oliveros RB (1998) 3-D sequence interpretation of seismic instantaneous attributes from the Gorgon Field. Lead Edge 17(9):1286–1293
Riedel M, Willoughby EC, Chopra S (2010) Geophysical characterization of gas hydrates. Society of Exploration Geophysicists, Tulsa
Roden R, Chen CW (2017) Interpretation of DHI characteristics with machine learning. First Break 35(5):55–63
Roden R, Smith T, Sacrey D (2015) Geologic pattern recognition from seismic attributes: principal component analysis and self-organizing maps. Interpretation 3(4):SAE59–SAE83
Roy A (2013) Latent space classification of seismic facies. Dissertation, University of Oklahoma
Sacrey D, Roden R (2014) Understanding attributes and their use in the application of neural analysis-case histories both conventional and unconventional. Search and Discovery Article 41473
Shuey RT (1985) A simplification of the Zoeppritz equations. Geophysics 50(4):609–614
Singh SC, Minshull TA, Spence GD (1993) Velocity structure of a gas hydrate reflector. Science 260(5105):204–207
Smith GC, Gidlow M (2003) The fluid factor angle and the crossplot angle. SEG Tech Prog Expand Abstr 2003:185–188
Spence GD, Haacke RR, Hyndman RD (2010) Geophysical characterization of gas hydrates. Society of Exploration Geophysicists, Tulsa
Subrahmanyam D, Rao PH (2008) Seismic attributes—a review. In: 7th international conference & exposition on petroleum geophysics, Hyderabad
Taner MT (2001) Seismic attributes. CSEG Recorder 26(7):49–56
Taner MT, Koehler F, Sheriff RE (1979) Complex seismic trace analysis. Geophysics 44(6):1041–1063
Turco F, Crutchley GJ, Gorman A, Mountjoy JJ, Hillman JIT, Woelz S (2020) Seismic velocity and reflectivity analysis of concentrated gas hydrate deposits on the southern Hikurangi Margin (New Zealand). Mar Petrol Geol 120:104572
Veeken PCH (2007) Seismic stratigraphy, basin analysis and reservoir characterization. Elsevier, Boston
Waite WF, Santamarina JC, Cortes DD, Dugan B, Espinoza DN, Germaine J, Jang J, Jung JW, Kneafsey TJ, Shin H, Soga K (2009) Physical properties of hydrate-bearing sediments. Rev Geophys 47(4):RG4003

Walsh MR, Hancock SH, Wilson SJ, Patil SL, Moridis GJ, Boswell R, Collett TS, Koh CA, Sloan ED (2009) Preliminary report on the commercial viability of gas production from natural gas hydrates. Energy Econ 31(5):815–823

Wood WT, Ruppel CD (2000) Seismic and thermal investigations of the Blake Ridge gas hydrate area: a synthesis. In: Proceedings of the Ocean Drilling Program, scientific results, Ocean Drilling Program, pp 253–264

Xu W, Ruppel C (1999) Predicting the occurrence, distribution, and evolution of methane gas hydrate in porous marine sediments. J Geophys Res Solid Earth 104(B3):5081–5095

Xu H, Dai J, Snyder F, Dutta N (2004) Seismic detection and quantification of gas hydrates using rock physics and inversion. In: Taylor CE, Kwan JT (eds) Advances in the study of gas hydrates. Springer, Boston, pp 117–139

Yoo DG, Kang NK, Bo YY, Kim GY, Ryu BJ, Lee K, Lee GH, Riedel M (2013) Occurrence and seismic characteristics of gas hydrate in the Ulleung Basin, East Sea. Mar Petrol Geol 47:236–247

Yun TS, Francisca FM, Santamarina JC, Ruppel C (2005) Compressional and shear wave velocities in uncemented sediment containing gas hydrate. Geophys Res Lett 32:10

Yun TS, Santamarina JC, Ruppel C (2007) Mechanical properties of sand, silt, and clay containing tetrahydrofuran hydrate. J Geophys Res Solid Earth 112:B4

Zhang L, Ge K, Wang J, Zhao J, Song Y (2020) Pore-scale investigation of permeability evolution during hydrate formation using a pore network model based on X-ray CT. Mar Pet Geol 113:104157